TIDAL FLAT EVOLUTION AT THE CENTRAL JIANGSU COAST, CHINA

Z. GONG

State Key Laboratory of Hydrology-Water Resources and Hydraulic Engineering, Hohai University, No.1, Xikang Road, Nanjing, 210098, China

Z.B. WANG

Deltares, P.O.Box 177, Delft 2600 MH, The Netherlands

Faculty of Civil Engineering and Geosciences, Delft University of Technology, P.O. Box 5048, Delft 2600 GA, The Netherlands

M.J.F. STIVE

Faculty of Civil Engineering and Geosciences, Delft University of Technology, P.O. Box 5048, Delft 2600 GA, The Netherlands

C.K. ZHANG

College of Harbor, Coastal and Offshore Engineering, Hohai University, No.1, Xikang Road, Nanjing, 210098, China

A schematized process-based model of tidal flat evolution was constructed with dimensions similar to the tidal flats near the Wanggang Mouth at the central coast of Jiangsu, China. The simulated flow patterns agree qualitatively with field observations from literature, i.e. involving tidal asymmetry, current directions and tidal wave features. The analysis of the sediment fluxes depicts that deposition occurs from spring tide to neap tide and erosion from neap tide to spring tide. A sensitivity analysis test of the morphological acceleration factor shows that the ideal value is only 1, implying no acceleration factor. The long-term mudflat evolution has been simulated starting from an initial sand seabed. The simulated morphological characteristics, including the convex cross-shore profiles with steeper slope and the southern prograding coastline with slight higher accretion rate compared with the north side, are qualitatively consistent with reality. Most importantly, the creek patterns are roughly reproduced.

1. Introduction

Tidal flats are characterized by rapidly varying water depth, both in time and space, including dry falling parts. These strong water level fluctuations induce

specific hydrodynamics, which in turn generate particular sediment processes [1]. However, the morphodynamics of mudflats, including the formation of mud bed forms, have been rather less studied than those of sandy beaches [2-3]. It is only in the last two decades that some field work on cohesive sediment properties, sediment transport mechanisms and mudflat morphology were carried out [4]. Empirical equilibrium profiles of mudflats and practical implications were proposed [5-7]. Simple mathematic models were built considering the effects of a cross-shore tidal current on filling and emptying intertidal flats [1, 8-9]. To first-order approximation, these models neglect fluid inertia, with velocities determined purely by fluid continuity. Consequently, tidal asymmetry can only be prescribed at open boundaries and internally generated tidal asymmetry cannot be reflected in these models. To overcome this limitation, Pritchard [2] built a morphological model for intertidal flats based on one-dimensional depth-averaged shallow water equations, considering fluid inertia but neglecting the effects of the long-shore current and associated sediment transport. We have extended this approach to two dimensions. On the basis of the 'sediment online' version of Delft3D, the process-based morphodynamic model of a schematized mudflat dominated by long-shore transport at the seaward boundary has been built in our study, with dimensions similar to the tidal flats near the Wanggang Mouth at the central coast of Jiangsu, China.

2. Area description

The study area is located in the middle part of Jiangsu coast, China (Figure 1). About 95% of the coast, between the Liezi Mouth and Qidong, is occupied by mud and silt tidal flats [10]. The tidal flats are unique in the world, in terms of their large scale and their offshore radial pattern with more than 70 submerged sand ridges [11-12]. The mudflats from the Sheyang Mouth to Jianggang, are the widest and fastest prograding mudflats in China [13]. The intertidal flats have a mean width of 2-6 km and a gradient of 0.01-0.03% [10, 13]. At the outer edge of the tidal flats, there is a wide, deep and shore-parallel tidal channel named the Xiyang Trough [13], which has a maximum depth of about 34m and is slightly eroding at present [14-15].

The Jiangsu sea area is controlled by a semi-diurnal tide. Two tidal wave systems, i.e. the East China Sea progressive tidal wave and the Southern Yellow Sea rotary tidal wave, converge near the coastal waters of Jianggang, generating a progressive wave in conjunction with a standing wave [16]. The tidal wave near the Wanggang Mouth has a mean tidal range of 3-4 m and propagates from northwest to southeast along the Xiyang Trough [17]. Maximum currents over the intertidal flats are ranging from 0.5-1.0 m/s.
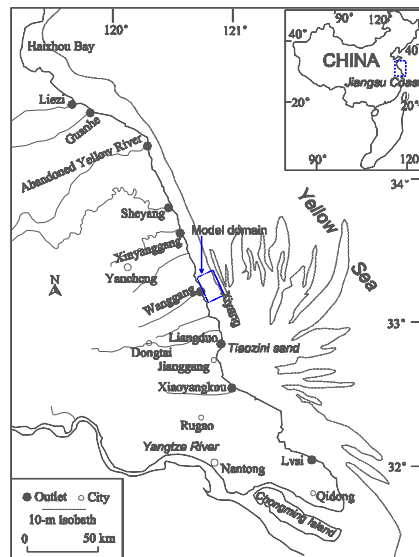
Figure 1. Locations of the tidal flats of Jiangsu coast and the model domain.
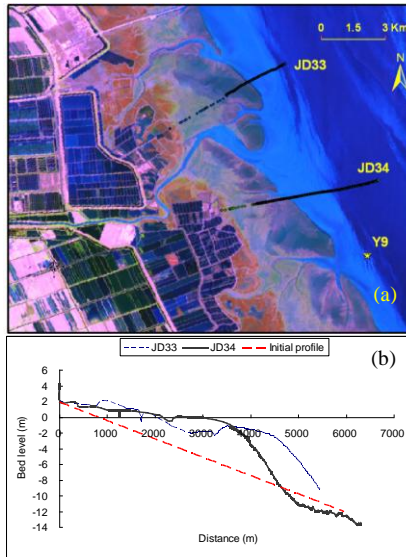
Figure 2. (a) Locations of the observation station Y9 and cross-sections JD33 and JD34. (b) Profiles JD33 and JD34 and the initial profile in the model.

The study area is sheltered by the offshore sand ridges, and only in autumn wind from the north has a large fetch [18]. Due to the wave energy attenuating on the long, shallow water mudflats, wave action is extremely weak [18, 19].

The sediment at the central coast is fine mud (i.e. a mixture of clay and silt) as a major sediment component [13]. The distribution of the surface sediment on intertidal flats shows trends of coarsening from the shore line towards the sea [13,18]. The observations near the Wanggang Mouth in 2008 show that the mud content decreases to 7.4% and the sand content increases to 92.6% on lower intertidal flats [18].

3. A process- based morphodynamic model implementation

3.1. *A process-based morphodynamic model*

This work uses the process-based model Delft3D for the integrated simulation of depth-averaged 2D flow, online coupling of sediment transport and morphological changes [20]. The total transport is calculated as the sum of suspended load transport and bed load transport [21]. The transport of cohesive sediment and sand-mud mixtures has been implemented by two regimes to calculate erosion fluxes of the mixed sand/mud sediment [22]. For sand fractions, the approach of van Rijn [21] is employed. For mud fractions, the

well-known Parthenaides and Krone formulations are adopted [23]. The online-morphology approach is used to run flow, sediment transport and bottom updating at identical computational time-steps [24].

3.2. *Model domain*

According to satellite images near the Wanggang Mouth, the tidal basin has a width of about 8 km along the coast [25] (Figure 2). The model domain is schematized as a rectangle of 8 km long-shore by 6 km cross-shore. With reference to the profiles of JD33 and JD34 surveyed in 2006 near the Wanggang Mouth, the initial cross-shore profile is schematized to be uniform along the coast and decreases seaward linearly from the elevation 2 m to -12 m (Figure 2).

3.3. *Open boundary conditions and major parameters*

On the basis of the harmonic constants of the Dafeng Harbor tide gauges during September, 2006 to October, 2007, the seaward boundary conditions are prescribed as harmonic water level series of M_2, M_4 and S_2 components, with amplitudes of 1.7 m, 0.2 m and 0.6 m, respectively. A Neumann hydrodynamic boundary condition is imposed on the lateral open boundaries [26].

The survey of 2006 shows that the median grain size (d_{50}) of suspended load in station Y9 (Figure 2) is 0.01 mm during flood current, and the cumulative mass percentage of sediment with a diameter more than 0.062 mm is up to 5%. Apparently, suspended cohesive sediment transport plays a much more important role than non-cohesive sediment. In the model, a suspended cohesive sediment concentration (SSC) is prescribed at the open boundaries.

The initial seabed is assumed to be composed of a 5 m mud layer and a 5 m sand layer with a grain size of 0.1 mm. The critical bed shear stress for erosion is 0.2 N/m². The settling velocity is 0.8 mm/s. The erosion coefficient is 2×10^{-4} kg/m²/s.

4. Results and discussion

4.1. *Selection of morphological acceleration factor*

First of all, a sensitivity analysis testing is carried out in order to select a suitable value of the morphological acceleration factor. Abundant sediment supply generally leads to deposition and insufficient sediment supply causes erosion. Thus, the morphological acceleration factors of these cases need to be analyzed respectively. The mass of available cohesive sediment, with a dry density of 500 kg/m³, is used to evaluate the suitability of morphological acceleration factors at two stations. One station is in the Xiyang Trough and the other is on lower

intertidal flats, with a distance from the shore of 4.5 km and 1.75 km, respectively.

For the first case with a boundary SSC condition of 1.05 kg/m^3, the mass of available cohesive sediment during 6375 hours (about 265 days) is shown in Figure 3. It shows that the larger the morphological acceleration factor (f) the larger is the difference of deposition in the Xiyang Trough. At the end of the simulation, the bed level simulated with f=5 differs more than 2 m from that simulated with f=1. On lower intertidal flats, the differences are much smaller. For the second case with a boundary SSC condition of 0.8 kg/m^3, it shows a similar distortion due to unsuitable morphological acceleration factors except for the strong erosion in the Xiyang Trough. Therefore, only a morphological acceleration factor of 1 (i.e. no morphological acceleration is acceptable) should be applied for the present model configuration.
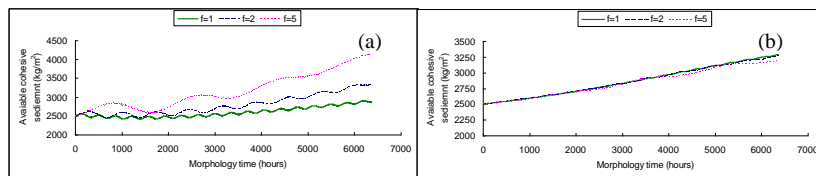
Figure 3. Available mass of cohesive sediment with different morphological acceleration factors for stations in the Xiyang Trough (a) and on lower intertidal flats (b).

4.2. *Initial patterns*

4.2.1. *Vertical and horizontal tide and sediment transport*

Three stations, P1, P2 and P3 in the middle cross-section with a distance of 6 km, 3 km and 1.5 km from the coast line respectively, are selected to analyze tidal asymmetry. After the bed evolution of 53 days with a boundary SSC condition of 0.8kg/m^3, started from an initial sand seabed similar to reality, the time series of water level, velocity magnitude, current direction and SSC are shown in Figure 4. Except at P3, situated on lower intertidal flats, exposed for about four hours during low water, the water levels are nearly identical. The duration of flood water is 72 minutes shorter than that of ebb water. Both flood current and ebb current decrease landwards. Maximum flood current is stronger than maximum ebb current. It can be concluded that the tide is flood dominant [18]. It is consistent with the observations in 2006, but opposite to the surveys in 1990's [14-15]. This may be induced by the change of tidal patterns and/or morphology in the past decades. Furthermore, the flood dominance is more significant landwards.
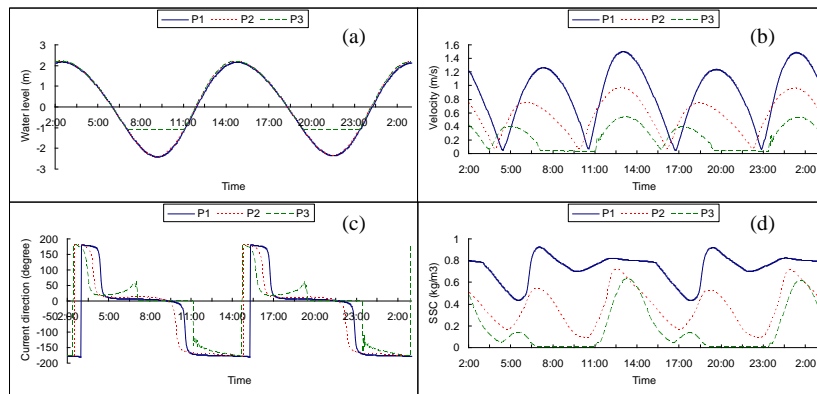
Figure 4. Water level (a), velocity magnitude (b), current direction (c) and SSC (d) of P1, P2 and P3.

For P1, there is a two hours phase difference between current and water level. Thus, the progressive tidal wave shows components of a standing wave. The tide in P2 shows a significant standing wave pattern. For P3, maximum flood current appears two hours later than the tide front [13, 17]. The current is rectilinear in the offshore channel, but is anti-clockwise rotary on the intertidal flats [13, 17-18]. The SSC decreases landwards. The variation of SSC closely follows that of the current. Maximum SSC is approximately in phase with the maximum current, but the phase of minimum SSC is one hour later than that of slack water [13, 17].

4.2.2. *Fluxes of suspended sediment*

For five days with uniform intervals in a fortnight tide cycle, after the bed evolution of 53 days from an initial sand seabed with a boundary SSC condition of 0.9 kg/m^3, the fluxes of suspended cohesive sediment at the open boundaries are calculated and shown in Figure 5, in which inflow fluxes are defined positive. The long-shore fluxes of suspended sediment are much larger than the cross-shore fluxes reflecting the dominance of a long-shore transport [18].

During the tide cycles from spring tide to neap tide, the fluxes of suspended sediment have decreasing trends, and the corresponding net fluxes increase from negative to positive. It means that the tidal flats evolve from erosion to deposition as a whole. During the tide cycles from neap tide to spring tide, the tidal flats evolve conversely.

4.3. *Long-term bed evolution with an initial sand seabed*

Surface sediment field observations and the comparisons of historic bottom topography prove that the sea bed in the Xiyang Trough is mainly composed of sand at present [14-15, 18]. To get close to reality, the initial seabed is assumed to be consisted of sand entirely. The boundary SSC condition of 0.8 kg/m^3 is imposed at open boundaries. The annual bed evolution of the middle cross-shore profile is shown in Figure 6. During first four years, sedimentation mainly occurs on intertidal flats. The plateau gradually fills up to the high water level of 2 m. After an equilibrium cross-shore profile is formed, the cross-shore profile keeps a convex shape and advances seaward with a speed of 250 m/yr as a whole, with slight erosion in the Xiyang Trough. Since the prograding of intertidal flats is faster than that of subtidal flats, the gradient of lower intertidal flats is higher than that of 0.3-0.4% in 1980's [27].

The depth evolution in the 9th year relative to mean sea level is shown in Figure 7. The accretion rate of the south cross-shore profile is slightly higher than that of the north profile. It is noteworthy that some creeks grow on upper intertidal flats and become organized progressively while running seaward. These creeks form a network of parallel ridges and creeks, cross-shore orientated. These patterns can also be observed in the Brouage mudflats as well as the Skeffling mudflats [3].
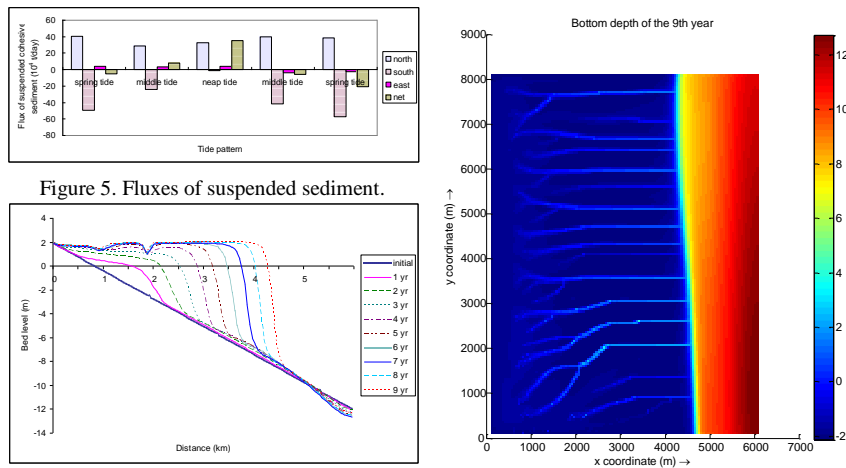
Figure 5. Fluxes of suspended sediment.
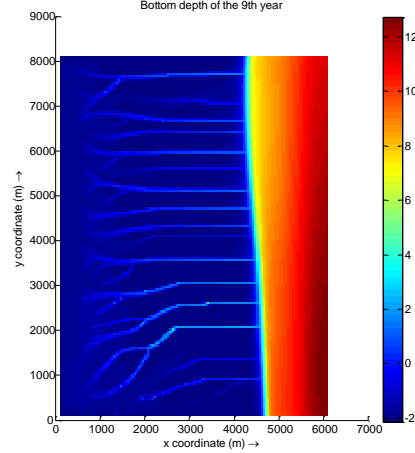
Figure 6. Annual bed evolution of the cross-shore profile.   Figure 7. Bottom depth in the 9th year.

5. Conclusions

A process-based morphodynamic model of a schematized mudflat dominated by long-shore transport at the seaward boundary has been built. Under the

conditions of a strong long-shore current, muddy seabed and SSC boundary conditions, the ideal morphological acceleration factor is only 1 (i.e. no acceleration). The simulated initial patterns agree qualitatively with field observations from literature. The long-term mudflat evolution has been simulated starting from an initial sand seabed. The simulated morphological characteristics are qualitatively consistent with reality. Most importantly, the creek patterns are roughly reproduced.

Acknowledgements

References

1. Le Hir, P., Roberts, W., *et al.*, *Continental Shelf Research.* **20** (12-13), 1433 (2000).
2. Pritchard, D., Hogg, A. J., *et al.*, *Continental Shelf Research.* **22** (11-13), 1887 (2002).
3. Whitehouse, R. J. S., Bassoullet, P., *et al.*, *Continental Shelf Research.* **20** (10-11), 1099 (2000).
4. Bassoullet, P., Le Hir, P., *et al.*, *Continental Shelf Research.* **20** (12-13), 1635 (2000).
5. Friedrichs, C.T., Aubrey, D.G., *Mixing in Estuaries and Coastal Seas.* 405 (1996).
6. Dyer, K.R., *Sedimentary Processes in the Intertidal Zone*. (1998).
7. Kirby, R., *Continental Shelf Research.* **20** (10-11), 1061 (2000).
8. Roberts, W., Le Hir, P., *et al.*, *Continental Shelf Research*, **20** (10-11), 1079 (2000).
9. Liu, X.J., Gao, S., *et al.*, *Earth Science-Journal of China University of Geosciences.* **35** (4), 542 (2010). (In Chinese).
10. Zhang, R.S., Shen, Y.M., *et al.*, *Ecological Engineering.* **23**, 95 (2004).
11. Wang, X.Y., Ke, X.K., *Sedimentary Geology.* **112**, 105 (1997).
12. Wang, Y., *Radiative sandy ridge field on continental shelf of the Yellow Sea*. (2002). (in Chinese).
13. Zhang, R.S., *Estuarine, Coastal and Shelf Science.* **35**, 225 (1992).
14. Zhu, D.K., Gong , W.P., *Marine science bulletin.* **13** (5), 36 (1994). (In Chinese).
15. You, K.Y., Zhu, D.K., *et al.*, *Geographical Research.* **17** (1), 10 (1998). (in Chinese).
16. Zhang, D.S., Zhang, J.L., *Journal of Hohai University.* **24** (5), 35 (1996). (in Chinese).

17. Ren, M.E., Zhang, R.S., Yang, J.H., *Marine Science Bulletin.* **3** (1), 40 (1984). (in Chinese).
18. Wang, Y.P., Gao,S.,*et al.*, *Marine Geology*. In Press, (2011).
19. Ren, M.E., etc, *Comprehensive investigation of coast zone and tidal flat resources, Jiangsu Province*. (1986). (in Chinese).
20. Lesser, G.R., Roelvink, J. A., *et al*., *Coastal Engineering.* **51**, 883 (2004).
21. Van Rijn, L. C., *Principles of sediment transport in rivers, estuaries and coastal seas*. (1993).
22. van Ledden, M., Wang, Z.B., *River, coastal and estuarine morphodynamics conference.* (2001).
23. Partheniades, E., *Journal of the Hydraulics Division*, ASCE **91** (HY 1). 105 (1965).
24. Roelvink, J.A., *Coastal Engineering*, **53** (2-3), 277 (2006).
25. Gong, Z., Zhang, C.K, *et al.*, *Proceedings of the 5th international conference on Asian and Pacific Coasts.* (2009).
26. Roelvink, J.A., Walstra, D.J.R., *6th international conference on Hydroscience and Engineering.* (2004).
27. Chen, C.J., *Oceanologia et Limnologia Sinica*, **22** (4), 360 (1991). (in Chinese).